Global Model of He/O_2 and Ar/O_2 Atmospheric Pressure Glow Discharges

Ganyoung Park, Hyunwoo Lee, Gyoocheon Kim, Jae Koo Lee*

Atmospheric pressure glow discharges (APGDs) have widespread applications, including sterilization, cancer cell treatment, deposition, and surface modification due to their rather simple configurations, thanks to no need for vacuum system and their great capability to generate reactive species such as radical oxygen species. Helium and argon are widely used as feeding gases, achieving stable operations for wide ranges of parameters in atmospheric pressure, and oxygen is added into these gases to generate more reactive oxygen species (ROS), which play a significant role in sterilization. As the measurements of species densities and electron temperature in APGDs are difficult, we have developed the zero-dimensional global model of He/O_2 and Ar/O_2 APGDs to calculate the densities of several kinds of species and electron temperature. It was shown that even though small fraction of oxygen less than 1% was added to helium or argon, electrons dissipated most of their energy through collisions with oxygen molecules rather than helium or argon atoms. The densities of electron, atomic oxygen, and ozone of Ar/O_2 were higher than those of He/O_2; however, the electron temperature of He/O_2 was higher than that of Ar/O_2. When the pulsed power is applied, the time-averaged electron temperature for the shorter pulse period and the larger duty ratio increased, and the electron density decreased as the duty ratio increased.

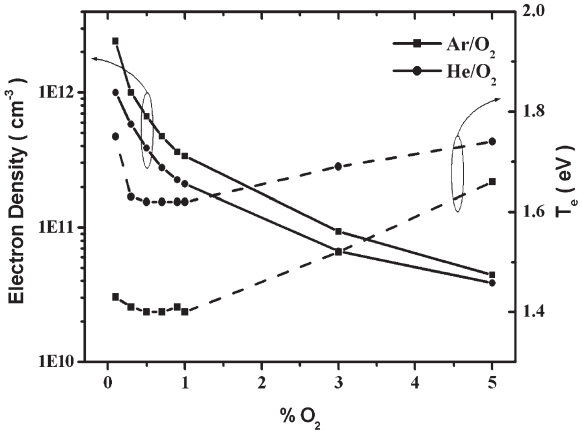

Introduction

Atmospheric pressure glow discharges (APGDs) have attracted great interests in the past decade because of their widespread applicability as well as their interesting physics. As APGDs have great advantages, which do not need expensive vacuum system, the absence of heat damage due to the operation in the nonthermal glow and the capability to produce agents such as reactive species, charged particles, and UV radiation, they are finding widespread applications including sterilization, cancer cell treatment, dental treatment, surface modification of biocompatible materials, and thin film deposition.[1,2] Various kinds of APGD sources such as the atmospheric pressure plasma jet, the dielectric barrier discharges, the atmospheric pressure plasma needle, and the cold plasma torch have been developed, and their generation has been

G. Park, H. Lee, J. K. Lee
Department of Electronic and Electrical Engineering, Pohang University of Science and Technology, Pohang 790-784, South Korea
Fax: (+82) 54 279 2903; E-mail: jkl@postech.ac.kr
G. Kim
Department of Oral Anatomy, College of Dentistry, Pusan National University, Busan 602-739, South Korea

DOI: 10.1002/ppap.200800019

achieved over a very wide spectrum from dc through kilohertz and megahertz to microwave, and their electrodes are either metallic or coated with a dielectric layer.[3–6]

As the measurements of species density and electron temperature in APGDs are difficult, we have developed the zero-dimensional global model[7] of He/O_2 and Ar/O_2 APGDs to calculate the densities of several kinds of species and electron temperature. Although the spatial information of the ionization rate, electric potential, and field is significant to understand the physics of APGDs through the fluid model[8] and particle-in-cell simulation[9] such as α and γ mode transition,[10] it is also important to comprehend their chemical reactions among several kinds of species because of the significant roles of reactive species in sterilizing bacteria and modifying material surface. We found the effects of the input power, the gas composition, the pulse period, and the duty ratio on electron temperature and densities of electron, ions, and radical species and made a comparison between He/O_2 and Ar/O_2 APGDs.

Model

The global model was widely used for analyzing low-pressure capacitively coupled discharges [7,11] and the hollow cathode.[12] This model has such advantages as very fast computational time and easy implementation for taking into account a number of species and reactions.

In the model of He/O_2 APGDs, 12 species, namely, electrons *e*, helium ions He^+, excited helium atoms He^*, dimer helium ions He_2^+, excited dimer He_2^*, positive oxygen molecule ions O_2^+, excited oxygen molecules $O_2(^1\Delta_g)$, ozone O_3, ground-state oxygen atoms $O(^3P)$, positive oxygen ions O^+, negative oxygen ions O^-, and excited oxygen atoms $O(^1D)$ are considered. Our model of He/O_2 includes 49 reactions for He/O_2 mixture selected from publications on discharge modeling in the literatures,[7,13–16] as listed in Table 1. The model of Ar/O_2 considers argon ions Ar^+, excited argon atoms Ar^*, and electrons *e* as well as species related to oxygen mentioned in the model of He/O_2. The reactions considered in the model of Ar/O_2 are listed in Table 2 and also include some reactions (R1-16, R27-44) in Table 1.

In an arbitrary volume, *V* enclosed by the surface area, *S*, the time-dependent particle balance equations for each species, indicating the balance between source and loss to result from the reactions among species and the wall loss due to the thermal diffusion are taken to be

$$\frac{d}{dt}(n_k) = (s_k - l_k) - \left(\frac{S}{V}\right)\Gamma_k, \quad (1)$$

where n_k is the density of species, s_k and $l_k$are the generation and loss rate due to the chemical reactions, respectively, and Γ_k is the flux into the boundary. Assuming the ions and radicals are Maxwellian distributions with the room temperature, the flux at the boundary is defined as

$$\Gamma_k = \frac{1}{4} n_k \bar{v}_k, \quad (2)$$

where $\bar{v}_k$ is the average velocity of species. The power balance equation meaning the balance between the input absorption power and the power loss of electrons due to the collisions with species is taken to be

$$\frac{d}{dt}\left(\frac{3}{2} n_e T_e\right) = P_{abs} - P_e \quad (3)$$

where T_e is the electron temperature in eV, P_{abs} the input power, and P_e is the power loss of electrons due to the chemical reactions. The types of the input power can be sinusoidal or pulsed. For the pulsed power, the rising time and falling time of the pulse are assumed to be zero. Equation (1) and (3) were solved simultaneously to calculate the species density and the electron temperature. It was assumed that as the model is a zero-dimensional one, all densities are spatially homogeneous. The densities of neutral species of helium, argon, and oxygen molecules are fixed at the initial values given by the fraction at the atmospheric pressure. The gas temperature was fixed at room temperature, 300 K, as the gas heating due to the collisions among feeding gases and other species was not considered.

Results and Discussion

Figure 1(a) and (b) shows densities of species in He/O_2 and Ar/O_2 atmospheric pressure discharges when the input power of 100 $W \cdot cm^{-3}$ applied to 1% O_2 admixture at the frequency of 13.56 MHz. The most dominant species are atomic oxygen and excited oxygen molecules in both discharges, which are known to be the bactericidal agents for sterilization.[17] It was shown that atomic oxygen and electrons in He/O_2 are slightly larger than those in Ar/O_2; however, helium ions are about one order of magnitude higher than argon ions. The powers dissipated by electrons through collisions with other species are shown in Figure 1(c) and (d). Even though 1% O_2 is added to helium and argon, electrons dissipated more than 90% of the absorbed power (100 $W \cdot cm^{-3}$ in these cases) through collisions with oxygen molecules and the dissipated power through collisions with helium or argon is less than 10%. Figure 1(e) and (f) shows the electron temperature calculated from this model. The electron temperature in He/O_2 is a little higher than that in Ar/O_2.

DOI: 10.1002/ppap.200800019

Table 1. A list of reactions for He/O_2 mixture.

No.	Reaction	Rate Constant	No.	Reaction	Rate Constant
		$cm^3 \cdot s^{-1}$			$cm^3 \cdot s^{-1}$
R1[a)]	$e + O_2 \rightarrow O_2 + e$	$4.7E - 8T_e^{0.5}$	R26[c)f)]	$e + O_2 + He \rightarrow O_2^- + He$	$1E - 31$
R2[a)]	$e + O_2 \rightarrow O_2^* + e$	$1.7E - 9\exp(-3.1/T_e)$	R27[a)]	$O^- + O_2^+ \rightarrow O + O_2$	$2E - 7(200/T)^{0.5}$
R3[a)]	$e + O_2^* \rightarrow O_2 + e$	$5.6E - 9\exp(-2.2/T_e)$	R28[a)]	$O^- + O \rightarrow O_2 + e$	$5E - 10$
R4[a)]	$E + O_2 \rightarrow O + O^* + e$	$5.0E - 8\exp(-8.4/T_e)$	R29[a)]	$O^- + O_2^+ \rightarrow 3O$	$1E - 7$
R5[a)]	$e + O \rightarrow O^* + e$	$4.2E - 9\exp(-2.25/T_e)$	R30[a)]	$O^- + O^+ \rightarrow 2O$	$2E - 7(300/T)^{0.5}$
R6[a)]	$e + O^* \rightarrow O + e$	$8E - 9$	R31[a)]	$O^+ + O_2 \rightarrow O + O_2^+$	$2E - 11(300/T)^{0.5}$
R7[a)]	$e + O^* \rightarrow O^+ + 2e$	$9E - 9T_e^{0.7}\ \exp(-11.6/T_e)$	R32[a)]	$O_2^* + O_2 \rightarrow 2O_2$	$2.2E - 18(T/300)^{0.8}$
R8[a)]	$e + O_2 \rightarrow O^- + O$	$8.8E - 11\ \exp(-4.4/T_e)$	R33[a)]	$O_2^* + O \rightarrow O + O_2$	$7E - 16$
R9[a)]	$e + O_2 \rightarrow 2O + e$	$4.2E - 9\ \exp(-5.6/T_e)$	R34[a)]	$O^* + O \rightarrow 2O$	$8E - 12$
R10[a)]	$e + O_2 \rightarrow O_2^+ + 2e$	$9E - 10T_e^{0.5}\ \exp(-12.6/T_e)$	R35[a)]	$O^* + O_2 \rightarrow O + O_2$	$7E - 12\exp(67/T)$
R11[a)]	$e + O^- \rightarrow O + 2e$	$2E - 7\exp(-5.5/T_e)$	R36[a)]	$O^* + O_2 \rightarrow O + O_2^*$	$1E - 12$
R12[a)]	$e + O_2^+ \rightarrow 2O$	$2.2E - 8T_e^{-0.5}$	R37[a)]	$O^- + O_2 \rightarrow O_3 + e$	$5E - 15$
R13[a)]	$e + O_2 \rightarrow O^- + O^+ + e$	$7.1E - 11T_e^{0.5}\ \exp(-17/T_e)$	R38[a)]	$O^- + O_2^* \rightarrow O_3 + e$	$3E - 10$
R14[a)]	$e + O_2 \rightarrow O + O^+ + 2e$	$5.3E - 10T_e^{0.9}\ \exp(-20/T_e)$	R39[a)]	$O^- + O_2^* \rightarrow O_2^- + O$	$1E - 10$
R15[a)]	$e + O \rightarrow O^+ + 2e$	$9E - 9T_e^{0.7}\ \exp(-13.6/T_e)$	R40[a)]	$O_3 + O_2 \rightarrow 2O_2 + O$	$7.3E - 10\exp(-11\ 400/T)$
R16[a)]	$e + O_3 \rightarrow O_2^- + O$	$1E - 9$	R41[a)]	$O_3 + O \rightarrow 2O_2$	$1.8E - 11\exp(-2\ 300/T)$
R17[b)]	$e + He \rightarrow He^* + e$	$4.2E - 9T_e^{0.31}\ \exp(-19.8/T_e)$	R42[d)f)]	$O + O + O_2 \rightarrow 2O_2$	$2.5E - 31T^{-0.63}$
R18[b)]	$e + He^* \rightarrow He + e$	$2E - 10$	R43[d)f)]	$O + O_2 + O_2 \rightarrow O_3 + O_2$	$6.9E - 34(300/T)^{1.25}$
R19[b)]	$e + He \rightarrow He^+ + 2e$	$1.5E - 9T_e^{0.68}\ \exp(-24.6/T_e)$	R44[d)]	$O_2^* + O_3 \rightarrow 2O_2 + O$	$6.0E - 11\exp(-2\ 853/T)$
R20[b)]	$e + He^* \rightarrow He^+ + 2e$	$1.28E - 7T_e^{0.6}\ \exp(-4.78/T_e)$	R45[b)]	$He^* + He^* \rightarrow He^+ + He + e$	$2.7E - 10$
R21[b)]	$e + He_2^* \rightarrow He_2^+ + e$	$9.75E - 10T_e^{0.71}\ \exp(-3.4/T_e)$	R46[b)f)]	$He^* + 2He \rightarrow He_2^* + He$	$1.3E - 33$
R22[b)]	$e + He_2^+ \rightarrow He^* + e$	$5E - 9T_e^{-0.5}$	R47[b)f)]	$He^+ + 2He \rightarrow He_2^+ + He$	$1E - 31$
R23[c)]	$e + He_2^+ \rightarrow He + He$	$1E - 8$	R48[c)f)]	$O + O + He \rightarrow O_2 + He$	$1.3E - 33(3\ 000/T)\exp(-170/T)$
R24[c)f)]	$e + He_2^+ + He \rightarrow 3He$	$2E - 27$	R49[e)]	$O_2^* + He \rightarrow O_2 + He$	$8E - 21$
R25[c)f)]	$e + e + He_2^+ \rightarrow 2He + e$	$5E - 27T_e^{-4.5}$			

Note. T_e in volts and T in Kelvins. O_2^* and O^* indicate $O_2^*(^1\Delta_g)$ and $O(^1D)$, respectively; [a)]ref. [6]; [b)]ref. [10]; [c)]ref. [11]; [d)]ref. [12]; [e)]ref. [13]; [f)]Rate constants are in $cm^6 \cdot s^{-1}$.

Table 2. A list of reactions for Ar/O_2 mixture.

No.	Reaction	Rate Constant	No.	Reaction	Rate Constant
		$cm^3 \cdot s^{-1}$			$cm^3 \cdot s^{-1}$
R1[a)]	$e + Ar \rightarrow Ar + e$	$3.9E - 13\exp(-4.6/T_e)$	R6[b)]	$O_2 + Ar^* \rightarrow O_2 + Ar$	$1.0E - 9$
R2[b)]	$e + Ar \rightarrow Ar^* + e$	$1.0E - 11T_e^{0.75}\ \exp(-11.6/T_e)$	R7[b)]	$O + Ar^* \rightarrow O + Ar$	$8.1E - 12$
R3[b)]	$e + Ar \rightarrow Ar^+ + 2e$	$4.0E - 12T_e^{0.5}\ \exp(-15.8/T_e)$	R8[b)]	$O_2 + Ar^* \rightarrow 2O + Ar$	$5.8E - 11$
R4[b)]	$e + Ar^* \rightarrow Ar^+ + 2e$	$2.05E - 7\exp(-4.95/T_e)$	R9[b)]	$O_2 + Ar^+ \rightarrow O_2^+ + Ar$	$1.2E - 11$
R5[c)]	$e + Ar^* \rightarrow Ar + e$	$2.0E - 7$	R10[b)]	$O + Ar^+ \rightarrow O^+ + Ar$	$1.2E - 11$

T_e in volts and T in Kelvins; [a)]ref.[15]; [b)]ref.[23]; [c)]ref.[24].

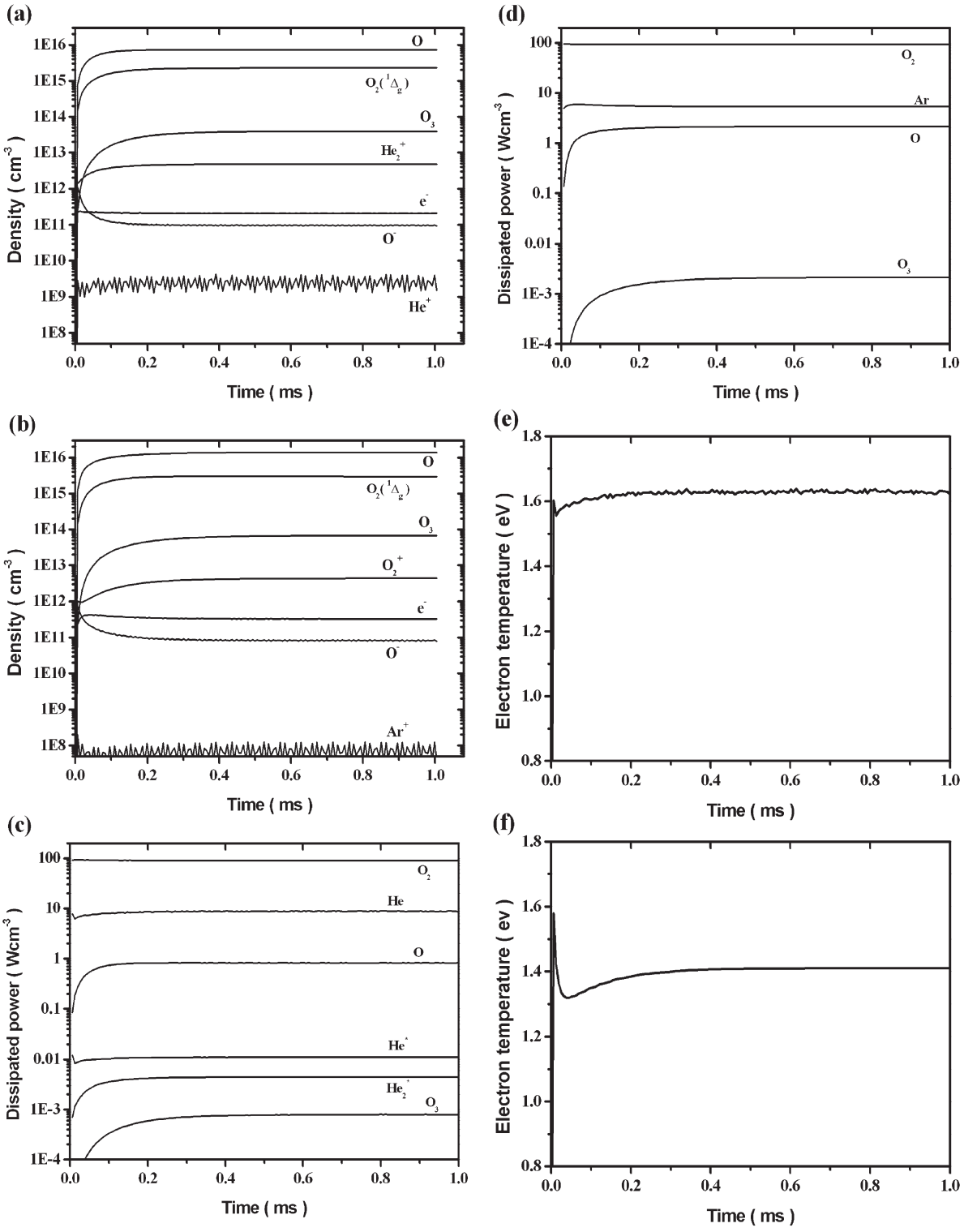

Figure 1. Densities of species of (a) He/O_2 and (b) Ar/O_2, power dissipated by electrons through other species of (c) He/O_2 and (d) Ar/O_2, and the electron temperature of (e) He/O_2 and (f) Ar/O_2 (Power = 100 W · cm^{-3}, f = 13.56 MHz and 1% O_2)

DOI: 10.1002/ppap.200800019

As the input power driven at 13.56 MHz increased from 0.1 to 1 000 $W \cdot cm^{-3}$, the density of electrons increased in both He/O_2 and Ar/O_2; however, the density of electrons in Ar/O_2 is higher than that in He/O_2 for those ranges of input power, as shown in Figure 2(a). This is due to the first lower excitation and ionization threshold energies (11.6 and 15.8 eV, respectively) of Ar than that (19.8 and 24.6 eV, respectively) of He.[18–20] Figure 2(b) shows the electron temperature while increasing the input power. As the input power increased to 10 $W \cdot cm^{-3}$, the electron temperature in both He/O_2 and Ar/O_2 decreased, then increased again as the power increased further. The electron temperature in He/O_2 is higher than that in Ar/O_2. It is shown in Figure 3 that the reactive oxygen species (ROS) density, such as atomic oxygen, ozone, and metastable oxygen, which play a significant role in plasma sterilization, increased as input power increased and those in Ar/O_2 are higher than those in He/O_2. The optical emission intensities of O (777.4 nm) and O (844.6 nm) were observed to be stronger in Ar/O_2 than in He/O_2, as the electron and the atomic oxygen density of Ar/O_2 are larger than that of He/O_2.[21]

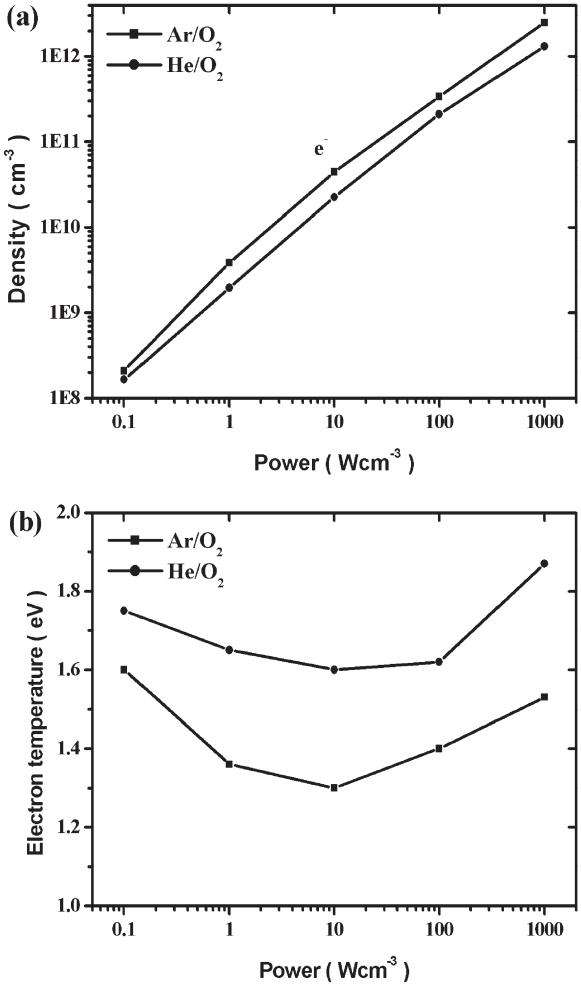

Figure 2. (a) The electron density and (b) the electron temperature of He/O_2 and Ar/O_2 for various input powers ($f = 13.56$ MHz and 1% O_2).

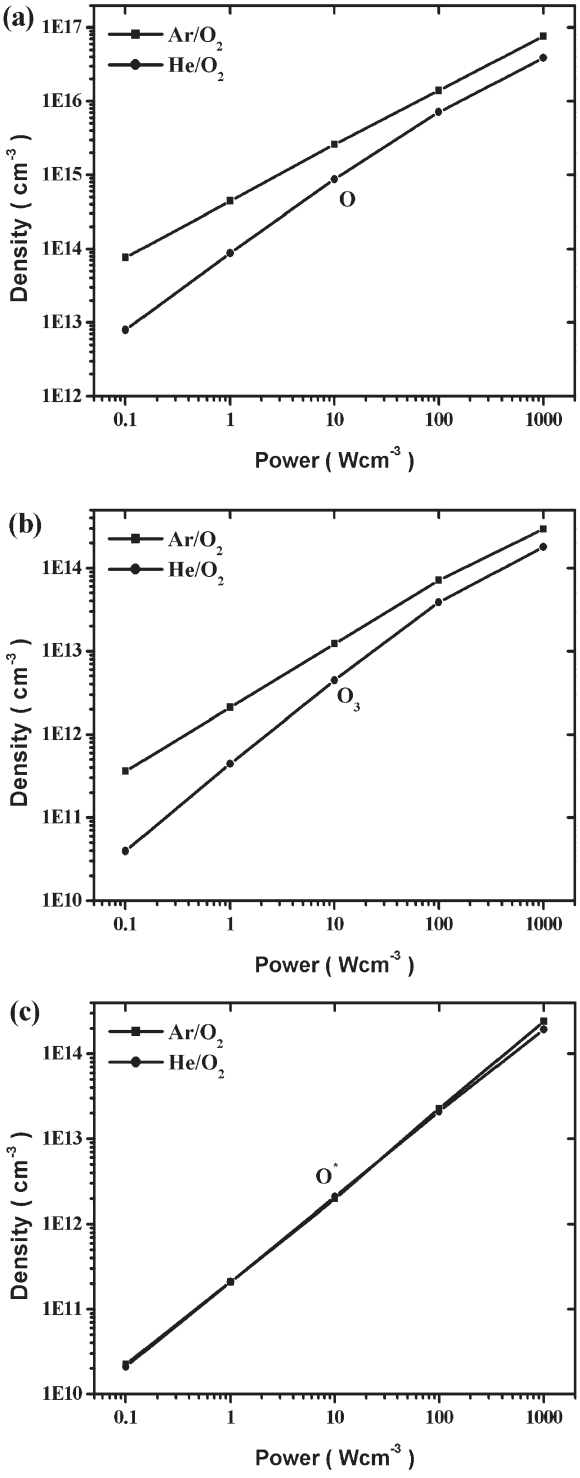

Figure 3. Densities of (a) atomic oxygen (b) ozone, and (c) metastable oxygen atom of He/O_2 and Ar/O_2 for various input powers ($f = 13.56$ MHz and 1% O_2).

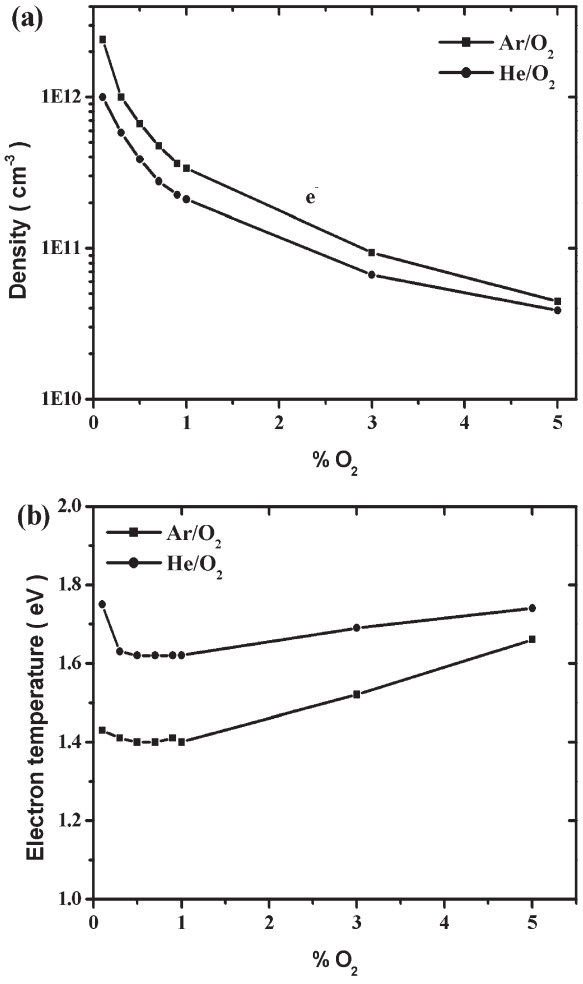

Figure 4. (a) The electron density and (b) the electron temperature of He/O_2 and Ar/O_2 for various fractions of oxygen (Power = 100 $W \cdot cm^{-3}$, $f = 13.56$ MHz).

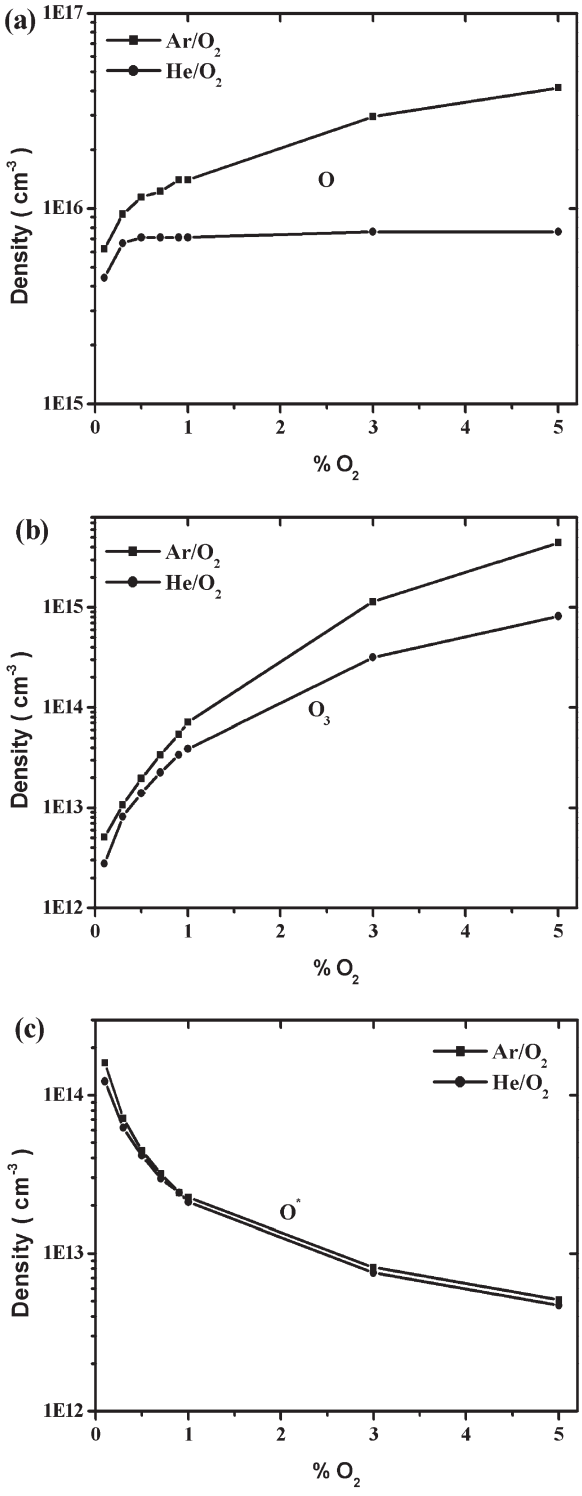

Figure 5. Densities of (a) atomic oxygen (b) ozone, and (c) metastable oxygen atom of He/O_2 and Ar/O_2 for various fractions of oxygen (Power = 100 $W \cdot cm^{-3}$, $f = 13.56$ MHz).

Figure 4 shows the electron density and temperature as the fraction of oxygen increased from 0.1 to 5.0% when the input power of 100 $W \cdot cm^{-3}$ was applied. The electron density decreased while increasing the fraction of oxygen, as oxygen is an electronegative gas and the attachment processes are loss channels of electrons. The electron temperatures of He/O_2 and Ar/O_2 were changed little when the fraction of oxygen was less than 1% except for the case of 0.1% in He/O_2; however, the electron temperature increased again while increasing the fraction of oxygen to 5%. The electron temperature of He/O_2 was higher than that of Ar/O_2 for those ranges of the fraction of oxygen. It is shown in Figure 5 that atomic oxygen and ozone of He/O_2 and Ar/O_2 increased, however, metastable oxygen atom decreased while increasing the fraction of oxygen. Although the electron density decreased as the fraction of oxygen increased, atomic oxygen and ozone of Ar/O_2 increased due to the increase in

DOI: 10.1002/ppap.200800019

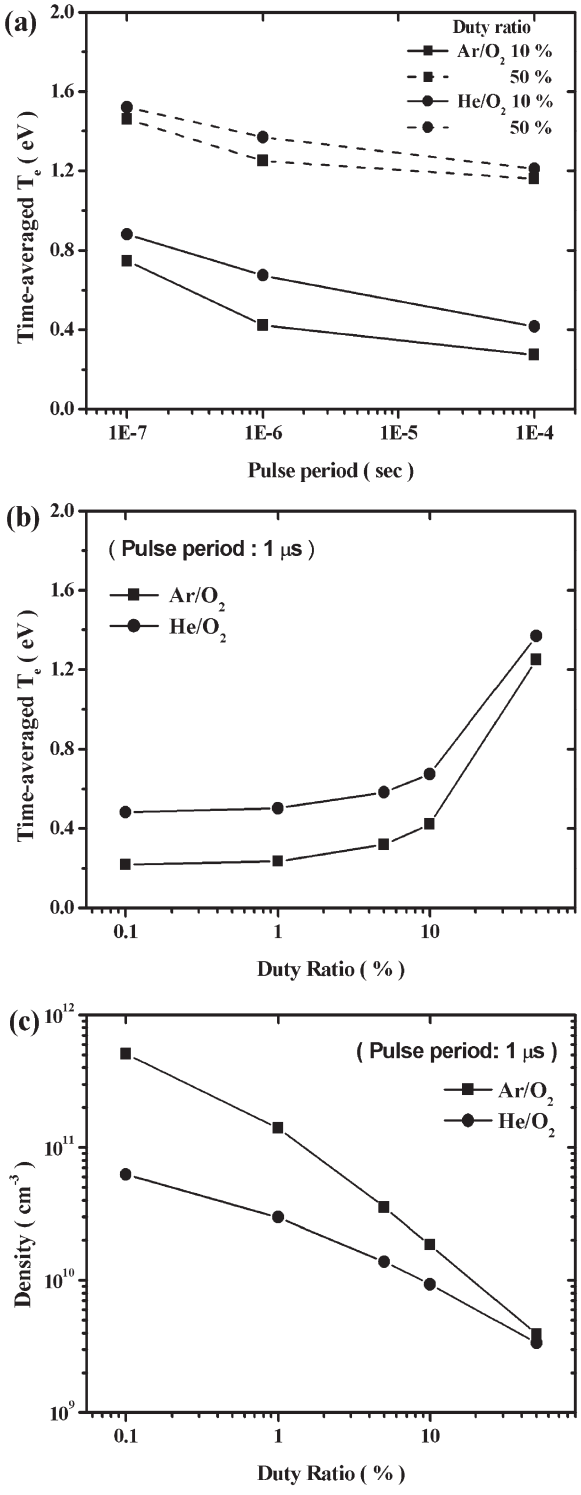

Figure 6. Time-averaged electron temperature T_e for (a) pulse period and (b) duty ratio, and (c) time-averaged electron densities for duty ratio (Averaged power = 1 $W \cdot cm^{-3}$ and 1% O_2).

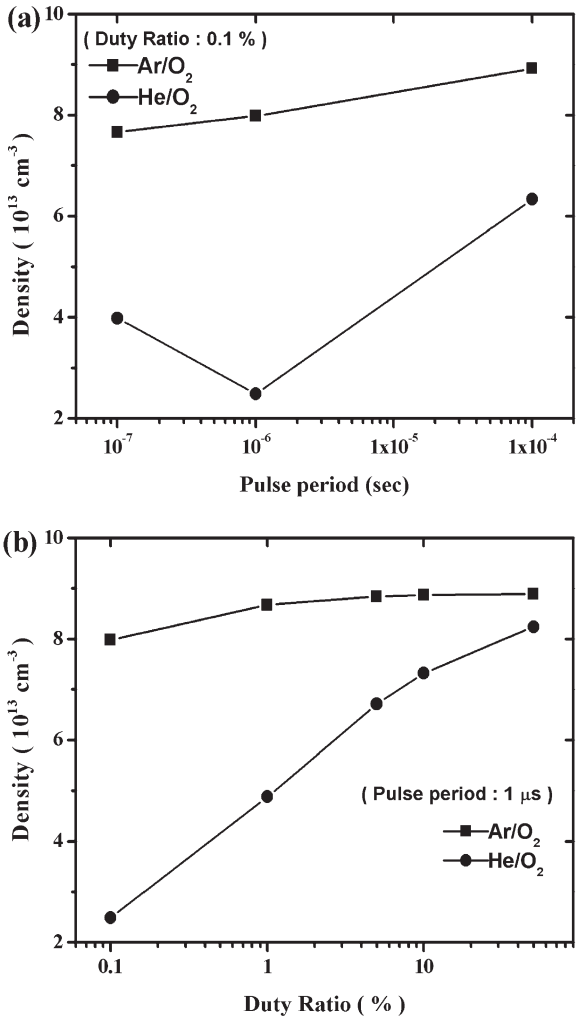

Figure 7. Time-averaged densities of atomic oxygen and metastable oxygen atom for (a) pulse period and (b) duty ratio (Averaged power = 1 $W \cdot cm^{-3}$ and 1% O_2).

the electron temperature, and atomic oxygen density of He/O_2 was saturated from the fraction of 0.3%. It was observed in ref. [22] that the optical emission intensity of O (777 nm) in He/O_2 discharges gradually decreased while increasing oxygen flow rate. This trend is similar to that of the metastable atomic oxygen, $O(^1D)$ rather than that of the atomic oxygen. The atomic oxygen and the ozone of Ar/O_2 are more abundant than those of He/O_2. This agrees with the result to show that Ar/O_2 is more efficient to sterilize bacteria than He/O_2.[21]

The effects of the pulse period and the duty ratio of DC-pulsed power on the electron temperature and densities of electron and several species when 1% of O_2 is added into argon or helium gas were investigated. The pulse period is a time interval between pulse trains. Time-averaged input power is kept at a constant value of 1 $W \cdot cm^{-3}$ on varying the peak value of pulse power density for different duty

ratios. For simplicity, the rising and falling time of the pulse were neglected.

The dependence of the time-averaged electron temperature on the pulse period and the duty ratio are shown in Figure 6(a) and (b). For the shorter pulse period and the larger duty radio, the time-averaged electron temperature increased because the electron temperature rapidly dropped nearly to zero during power off period. The similar results were shown in ref.[11]. The time-averaged electron temperature of He/O_2 is higher than that of Ar/O_2. Figure 6(c) shows the time-averaged electron density on varying the duty ratio. The electron density decreased as the duty ratio increased and the electron density of Ar/O_2 is higher than that of He/O_2.

It was shown in Figure 7(a) and (b) that the densities of atomic and excited oxygen of Ar/O_2 increased as the pulse period and the duty ratio increased, however, those of He/O_2 had minima at the pulse period of 10^{-6} s, and they also increased as the duty ratio increased.

Conclusion

It is important to estimate the densities of the excited and reactive species that play crucial roles to sterilize bacteria for different input powers and fractions of O_2 admixture. To do that, we have developed zero-dimensional global models of He/O_2 and Ar/O_2 APGDs solving time-dependent particle and power balance equations simultaneously. It was observed that the atomic oxygen and the excited oxygen molecule are the most dominant species even in the admixture of 1% O_2. It was shown that even though small fraction of oxygen less than 1% was added to helium or argon, electrons dissipated most of the absorbed energy through collision reactions with oxygen molecules rather than helium or argon atoms. As the admixture of oxygen increased, the electron density decreased due to the loss channel resulting from the attachment reaction processes, and the electron temperature slightly increased. The densities of electron, atomic oxygen, and ozone of Ar/O_2 are higher than those of He/O_2; however, the electron temperature of He/O_2 is higher than that of Ar/O_2. When the pulsed power is applied, the time-averaged electron temperature for the shorter pulse period and the larger duty radio increased, and the electron density decreased as the duty ratio increased. Using this model, we could understand the characteristics of APGDs quantitatively and qualitatively.

Acknowledgements: The authors are grateful to Dr. *P. K. Tiwari* for his comments. This work was supported by the Korea Science and Engineering Foundation (KOSEF) grant funded by the *Korea Government* (MOST) (No. R01-2007-000-10730-0) and the *Korea Ministry of Education* though its Brain Korea 21 program.

Received: January 31, 2008; Revised: April 29, 2008; Accepted: May 16, 2008; DOI: 10.1002/ppap.200800019

Keywords: atmospheric pressure glow discharge (APGD); atomic oxygen; computer modeling; density; global model; reactive oxygen species (ROS)

[1] M. Laroussi, *Plasma Process Polym.* **2005**, *2*, 391.
[2] G. Fridman, A. Shereshevsky, M. M. Jost, A. D. Brooks, A. Fridman, A. Gutsol, V. Vasilets, G. Friedman, *Plasma Chem. Plasma Process* **2007**, *27*, 163.
[3] F. Iza, G. J. Kim, S. M. Lee, J. K. Lee, J. L. Walsh, Y. T. Zhang, M. G. Kong, *Plasma Process Polym.* **2008**, *5*, 322.
[4] M. Laroussi, T. Akan, *Plasma Process Polym.* **2007**, *4*, 777.
[5] E. Stoffels, I. E. Kieft, R. E. J. Sladek, *J. Phys. D: Appl. Phys.* **2003**, *36*, 2908.
[6] V. Leveille, S. Coulombe, *Plasma Sources Sci. Technol.* **2005**, *14*, 467.
[7] M. A. Lieberman, A. J. Lichtenberg, "*Principle of Plasma Discharges and Materials Processing*", Wiley, New York 2005.
[8] Y. B. Golubovskii, V. A. Maiorov, J. Behnke, J. F. Behnke, *J. Phys. D: Appl. Phys.* **2003**, *36*, 39.
[9] F. Iza, J. K. Lee, M. G. Kong, *Phys. Rev. Lett.* **2007**, *99*, 075004.
[10] J. J. Shi, M. G. Kong, *Phys. Rev. Lett.* **2006**, *96*, 105009.
[11] S. J. Kim, M. A. Lieberman, A. J. Lichtenberg, J. T. Gunmundsson, *J. Vac. Sci. Technol., A* **2006**, *24*, 2025.
[12] H. J. Lee, J. K. Lee, *Jpn. J. Appl. Phys.* **1996**, *35*, 6252.
[13] X. Yuan, L. L. Raja, *IEEE Trans. Plasma Sci.* **2003**, *31*, 495.
[14] K. R. Stalder, R. J. Vidmar, G. Nersisyan, W. G. Graham, *J. Appl. Phys.* **2006**, *99*, 093301.
[15] M. Moravej, X. Yang, R. F. Hicks, J. Penelon, S. E. Babayan, *J. Appl. Phys.* **2006**, *99*, 093305.
[16] J. Y. Jeong, J. Park, I. Henins, S. E. Babayan, V. J. Tu, G. S. Selwyn, G. Ding, R. F. Hicks, *J. Phys. Chem., A* **2000**, *104*, 8027.
[17] S. Perni, G. Shama, J. L. Hobman, P. A. Lund, C. J. Kershaw, G. A. Hidalgo-Arroyo, C. W. Penn, X. T. Deng, J. L. Walsh, M. G. Kong, *Appl. Phys. Lett.* **2007**, *90*, 073902.
[18] S. Wang, V. Schulz-von der Gathen, H. F. Dobele, *Appl. Phys. Lett.* **2003**, *83*, 3272.
[19] S. Z. Li, J. P. Lim, J. G. Kang, H. S. Uhm, *Phys. Plasmas* **2006**, *13*, 093503.
[20] M. Moravej, X. Yang, G. R. Nowling, J. P. Chang, R. F. Hicks, S. E. Babayan, *J. Appl. Phys.* **2004**, *96*, 7011.
[21] J. P. Lim, H. S. Uhm, S. Z. Li, *Phys. Plasmas* **2007**, *14*, 093504.
[22] W. Bairong, Z. Wenchao, P. Yikang, *Plasma Sci. Technol.* **2005**, *7*, 3045.
[23] C. Lee, M. A. Lieberman, *J. Vac. Sci. Technol. A* **1995**, *13*, 368.
[24] M. H. Lee, C. W. Chung, *Phys. Plasmas* **2005**, *12*, 073501.